Received July 1, 2014, accepted July 14, 2014, date of publication September 23, 2014, date of current version October 8, 2014.

Digital Object Identifier 10.1109/ACCESS.2014.2359996

Reluctance Accelerator Efficiency Optimization via Pulse Shaping

LIAM M. COOPER[1,2], ABIGAIL R. VAN CLEEF[1,3], BERNARD T. BRISTOLL[1], AND PAUL A. BARTLETT[1]

[1]Department of Physics and Astronomy, University College London, London WC1E 6BT, U.K.
[2]Accenture, London EC4M 7AN, U.K.
[3]Grant Thornton UK LLP, London EC2P 2YU, U.K.

Corresponding author: P. A. Bartlett (paul.bartlett@ucl.ac.uk)

ABSTRACT Reluctance accelerators are used to apply linear forces to ferromagnetic projectiles via solenoids. Efficiency increases for a single-stage reluctance accelerator were produced by manipulating the input current pulse supplied by a discharging capacitor. The development of a theoretical model allowed for the calculation of optimized pulse shapes. A digital pulsewidth modulated switching method was used to control the current pulse shape using an Arduino Uno microcontroller, which supplied signals to the gate of a MOSFET transistor that controlled the current to the system solenoid. An efficiency increase of 5.7% was obtained for a reluctance accelerator with an optimized current pulse shape in comparison to a capacitor discharge with no pulse shaping.

INDEX TERMS Reluctance accelerators, electromagnetic launchers, linear accelerators, pulse shaping.

I. INTRODUCTION

Reluctance accelerators are a class of linear motor that can be used to accelerate ferromagnetic objects with lower drive currents than other induction machines [1]. In a reluctance accelerator, a current pulse is applied to a stator solenoid that generates a transient magnetic-field. This field induces an accelerating force on a positioned ferromagnetic projectile. It is called a reluctance accelerator as the force acting on the projectile moves it to the location of minimum magnetic-reluctance [2].

A reluctance accelerator consists of either a single or series of stator solenoids. A single solenoid is configured coaxially with a ferromagnetic projectile so that applying a current pulse to the solenoid accelerates the projectile towards its center due to the induced magnetic field [3]. A series of solenoids can accelerate a projectile from the resultant magnetic forces of sequential current-pulses applied to each solenoid.

Reluctance can be considered to be the magnetic equivalent to resistance in electrical circuits. The magnetic flux (ϕ) flowing in a circuit, due to the application of a magnetomotive force (m.m.f), is determined by reluctance ($\Re$) so that [1]

$$\Re = m.m.f/\phi = l/\mu_0\mu_r A \tag{1}$$

where μ_0 is the permeability of free space, μ_r is the relative permeability of the material within the magnetic field, l is the length of the flux-path and A is the cross-sectional area of the solenoid core. The $m.m.f$ for a stator solenoid based system can be approximated by

$$m.m.f = NI \tag{2}$$

where N is the number of turns for the solenoid and I is the current flowing through it.

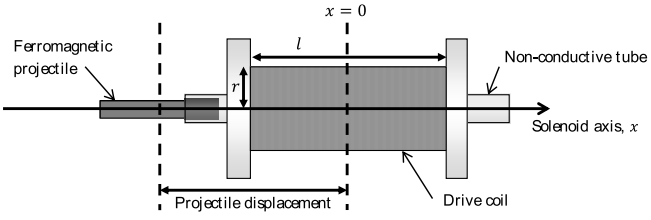

FIGURE 1. Schematic diagram of single solenoid reluctance accelerator displaying the main system components. It shows the position and direction of motion of a ferromagnetic projectile, prior to application of an accelerating pulse, at a distance from the solenoid center (at x = 0).

A single-stage reluctance accelerator consists of one stator solenoid, known as a drive coil, to accelerate a ferromagnetic projectile. A schematic of such a system is shown in Fig. 1. The projectile is initially positioned, as shown in Fig.1, at a displacement x away from the center of the solenoid.

When a current pulse is applied to the drive coil, a transient magnetic-field is created that applies a force to the ferromagnetic projective, drawing it to the center of the coil. The current pulse is, typically, supplied by a capacitor that is discharged through the drive coil at a rate determined by the time constant of the entire system. The reluctance of the system will change, as the projectile moves, until it achieves a minimum reluctance (for a given flux level) when the center of the projectile coincides with the center of the solenoid [2]. Once the accelerated projectile moves past the point of minimum reluctance, the net restoring force acts to return the projectile to this point. This effect is known as 'suck-back' and is undesirable as it opposes the desired direction of motion and reduces the resultant exit velocity of the projectile from the accelerator system. Consequently, it is important to terminate the magnetic field-pulse once the projectile reaches the point of minimum reluctance to optimise the efficiency (η) of the system in converting the electrical energy supplied to the solenoid (U) to projectile kinetic energy ($K.E.$) [1]

$$\eta = \frac{K.E.}{U} = \frac{mu_{exit}^2}{C(V_{before}^2 - V_{after}^2)} \tag{3}$$

where m is the mass of the projectile, u_{exit} is the velocity of the projectile after leaving the acceleration system, C is the capacitance of the capacitor that supplies the current pulse and V_{before} and V_{after} are the potential differences (p.d) measured across the capacitor before and after discharge. It has been identified [1], [4] that reluctance accelerators are relatively inefficient devices with efficiencies of $\sim$2% for optimised systems. It must be noted that this value is influenced by properties such as saturation magnetization of the armature, coil losses, eddy-current losses and geometric factors.

II. SYSTEM COMPONENTS

To investigate the performance of reluctance accelerator systems, a single-stage device was constructed as seen in Fig.2.

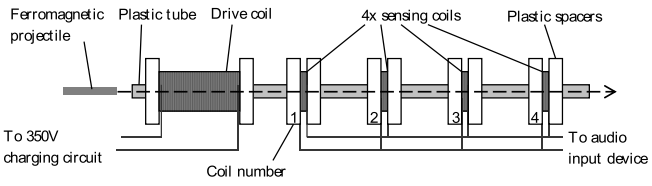

FIGURE 2. Schematic diagram of single solenoid reluctance accelerator with four sensing coils to determine the ferromagnetic projectile velocity. The magnetic field of the projectile induces a pulse in each sensing coil due to the projectile motion. The drive coil is connected to a circuit that supplies current from a charged capacitor.

The reluctance accelerator system comprised of an accelerating 'drive coil' and four sensing coils all mounted on a central fiberglass tube. The device parameters are shown in Table 1. This system used a soft ferromagnetic Maximag projectile. The high-purity soft-iron material was desirable to avoid magnetisation saturation which results in efficiency reduction. This projectile was used in all experiments so that relative increases or decreases in system efficiency could be identified.

TABLE 1. Reluctance accelerator component parameters.

Component	Parameters
Drive coil	520 turns (30±0.25)mm length (7.0±0.25)mm outer diameter (0.50±0.010)mm enamel-coated copper wire
Sensing coils	200 turns (1.50±0.010)mm (0.20±0.010)mm enamel-coated copper wire
Sensor-coil separation	1-2: (0.031±0.0010)mm 2-3: (0.034±0.0010)mm 3-4: (0.030±0.0010)mm
Fiber-glass launch tube	(175±0.25)mm x (7.0±0.01)mm (7.0±0.25)mm outer diameter (4.0±0.25)mm internal diameter (25±0.25)mm length (3.62±0.005)mm diameter
Maximag® projectile	Mass: (2.026±0.0005)g
Storage Capacitor	82µF 400V

A charged capacitor was selected to deliver a current pulse to the drive coil. This component discharges with an exponential decay, which is suitable to supply a high current in a short pulse. The rate of discharge depends on the time constant of the discharge circuit.

$$I(t) = I_0 e^{-t/RC} \tag{4}$$

where $I(t)$ is time-dependent current, I_0 the initial current upon discharge, R is the circuit resistance and C is the capacitance of the storage capacitor.

As the ferromagnetic projectile passes the four sensing coils, an electromagnetic pulse is induced in each coil. The velocity of the passing projectile is calculated from the induced pulses. This was achieved by recording the electromagnetic pulses via the audio input-port of a computer and processing the waveform with a Java program written for this purpose.

III. INITIAL TRIGGER-CIRCUITRY

To supply current pulses from the charged capacitor, a trigger circuit was designed so that a solid-state switch could be used to control the discharge. A Fairchild FDL100N50F, 'N-Channel', 500V, 100A MOSFET was used to control the current pulse delivered to the drive coil (see Fig.3).

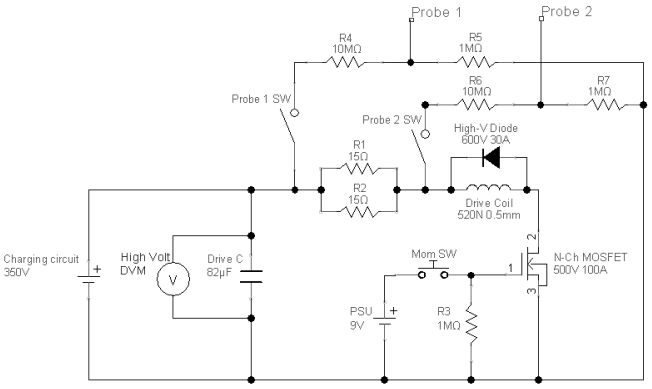

FIGURE 3. Triggering circuit used to control the supply of current from the storage capacitor (shown here as 'Drive C 82 μF') to the drive coil by applying a voltage to the gate of a MOSFET transistor.

The potential difference (p.d). across the capacitor was measured using a digital storage oscilloscope (DSO) via attenuator resistors shown in Fig.3 (Probe 1 and 2). The two 15Ω 7W ceramic resistors, R1 and R2, were connected in parallel before the drive coil to limit the peak current output across the trigger circuit. This ensured that all the selected components do not operate outside the stated limits. Although they could reduce the efficiency of the system, the experiments sought to see how relative efficiencies could be increased through pulse-shaping.

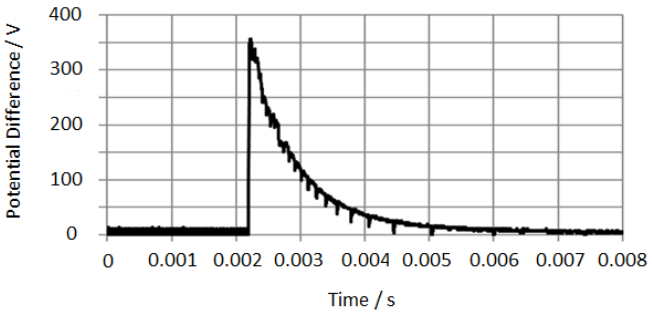

FIGURE 4. The complete decay of the p.d. across the storage capacitor over time, initially charged to (350±0.5)V, as it discharged through the drive coil.

The decay of the capacitor p.d. is shown in Fig. 4.

IV. OPTIMAL STARTING POSITION

Initial experimentation established the optimum starting position of the projectile of a complete capacitor discharge. Exit velocities were recorded for a range of initial projectile positions, from −11.5mm to −20.5mm shown in Fig. 5. Initial projectile positions were measured from the centre of the drive coil (0mm), with positive displacements following the direction of motion when accelerated. The peak exit velocity (3.84 ± 0.04) ms^{-1} was recorded for an optimum initial projectile position of −15.5mm. This optimised starting position minimised the influence of 'suck-back' on the projectile for a complete capacitor discharge, (charged to (350 ± 0.5)V).

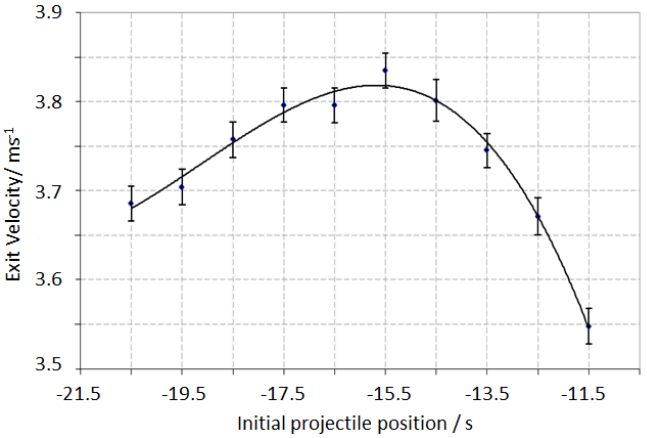

FIGURE 5. The effect of the change in exit velocity for a range of initial projectile positions, using an unaltered capacitor current pulse charged to (350±0.5)V.

V. PULSE TRUNCATION

Further experiments were undertaken to investigate whether truncating the current pulse could assist in reducing the influence of suck-back.

To achieve these truncated pulses, the manual trigger circuit in Fig.3 was replaced by an Arduino Uno microcontroller that sent control signals to the gate of the MOSFET via a MOSFET driver (Microchip TC4428 1.5A High-Speed Power Driver). The modified circuit can be seen in Fig. 6.

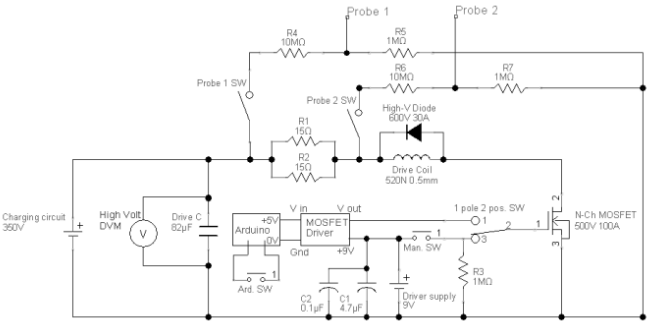

FIGURE 6. Triggering circuit used to control the supply of current from the capacitor (shown here as 'Drive C 82 μF') to the drive coil by applying a control signal from an Arduino Uno microcontroller to the gate of a MOSFET via a MOSFET driver. The ability to manually trigger the MOSFET via a switch was retained in this system.

Fig. 7 shows an example of a simple truncated capacitor discharge, produced from the circuit in Fig. 6.

Using the Arduino, it was possible to truncate pulses using a switching precision of (0.021±0.01)ms. The efficiency over a range of truncated current pulses, compared against the 'baseline' efficiency, is shown in Fig. 8. The 'baseline' efficiency is noted as the efficiency of the system for a full capacitor discharge with no current-pulse manipulation.

The maximum efficiency achieved with the system using pulse truncation was (0.32 ± 0.02)% using a 2500 μs pulse duration. Although this is a low efficiency, this was a relative increase of 3.7% compared to an unaltered current

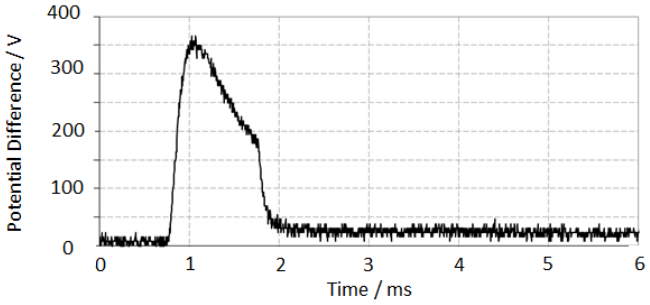

FIGURE 7. The decay of the p.d. across the storage capacitor, initially charged to (350±0.5)V, as it discharged through the drive coil. The decay was truncated to a ∼ 1ms current pulse by switching the MOSFET using the Arduino Uno.

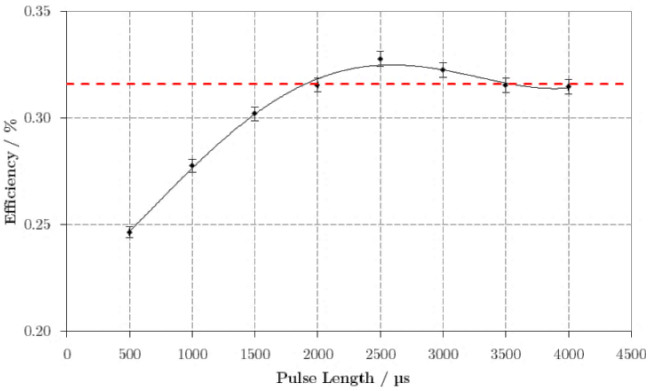

FIGURE 8. The change in efficiency for a range of truncated capacitor pulse durations, charged to (350±0.5)V, to display the effect of 'suck-back'. Initial projectile position: (−15.5±0.05)mm. The dotted line shows the efficiency of the system without pulse truncation, the 'baseline' efficiency.

pulse. The efficiency increases gained from this were due to further reductions in the 'suck-back' effect. In addition, this method of efficiency gains can be used if the starting position of the projectile is not efficiency optimized.

VI. PULSE SHAPING VIA PULSE WIDTH MODULATION TECHNIQUES

The Arduino Uno was programmed using precompiled Java code, to run a variety of functions to control the MOSFET. A proposed method of operation was to control the microcontroller by a computer or another device using the microcontroller's Serial Peripheral Interface (SPI). The computer would process a mathematical input pulse function and send the information in real-time. However, this was not viable due to the insufficient rate of data transfer for current-pulse control (maximum of 1M Serial Baud Rate [7]). Flashing the device with an input pulse function avoided any data transfer delays, but introduced processing delays of the microcontroller. Initial testing found that uploading mathematical input pulse functions to the Arduino Uno halved the output voltage resolution in comparison to that with no data processing. Therefore, all mathematical functions were pre-processed and uploaded to the microcontroller as an integer-array list.

The modification of the current pulse shape applied to the drive coil was investigated for further potential efficiency gains.

This was achieved by applying high-frequency Pulse Width Modulated (PWM) signals to the MOSFET so that the capacitor discharge rate could be varied over the pulse duration. The Arduino Uno contains a ATMega328 processor that has the ability to supply PWM signals with a frequency up to 62.5kHz. It is common to supply PWM signals to motors [6] where the inductor/resistor network associated with the solenoid would act as a low-pass filter. This removes the high-frequency components of the PWM signal leaving a voltage that is dependent on the duty cycle (with 256 possible increments) of the PWM signal applied to the solenoid/MOSFET circuit. As the drive coil is in series with the drain-source path, this means that the PWM p.d. applied to the MOSFET gate will control the effective resistance of the system and the resultant current pulse across the drive coil.

The characteristics of a N-type MOSFET transistor allow it to act as a voltage dependent resistor when it is operated in the 'linear' mode [8]. Consequently, the Arduino-generated PWM signal can be used as the input gate to source voltage to control the effective resistance of the path from the capacitor supply, through the coil and on through the MOSFET.

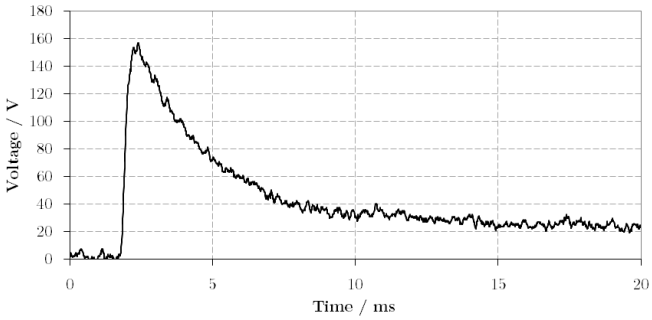

FIGURE 9. Potential difference across the drive coil for an Arduino Uno PWM (40% duty cycle) signal applied to the MOSFET gate. The increase in 'effective resistance' of the reluctance accelerator system reduces the peak discharge p.d. form 350 V to 150 V, showing how PWM signals can control pulse shapes.

This control can be seen in Fig. 9 where an Arduino Uno PWM signal has reduced the peak p.d. across the drive coil from 350V to 150V.

The effective resistance for a range of PWM duty cycles was measured to obtain an 'effective resistance' profile (see Fig. 10). The effective resistance was calculated by measuring the p.d. across the drive coil and using the time constant of the system. This profile could then be used to produce the desired circuit resistance to alter the capacitor discharge on the drive coil from an input PWM signal with varying duty cycles.

A Mathematica based theoretical model was produced to calculate efficiency optimized current pulse shapes. The Mathematica model produced theoretical time-dependent resistance functions of the discharge circuit. The 'effective

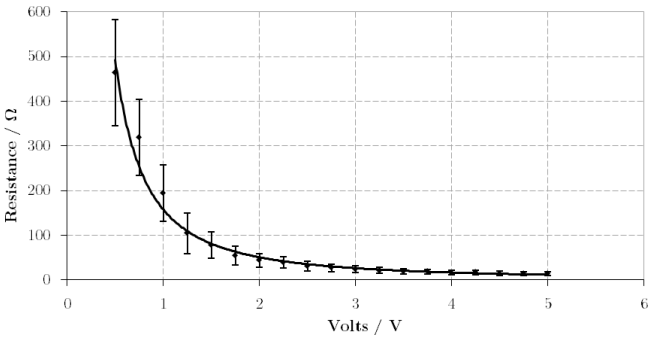

FIGURE 10. Effective resistance of the reluctance accelerator discharge circuit vs. the Arduino Uno PWM signal applied to the MOSFET gate where 5V equates to a 100% duty cycle.

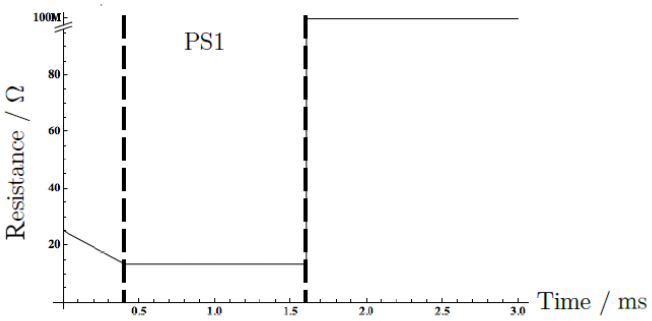

FIGURE 11. Theoretical model, 'Pulse Shape 1' (PS1), generated three-stage profile, derived from transforming the theoretical efficiency optimized output resistance function with the resistance profile.

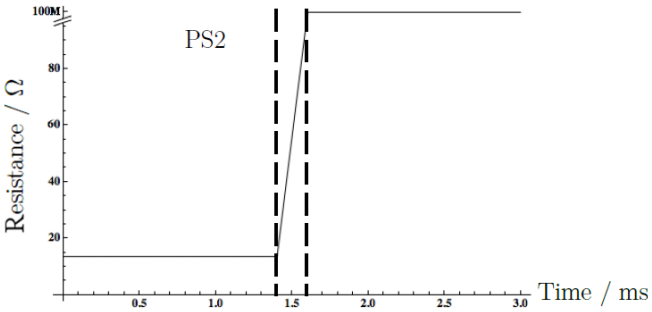

FIGURE 12. Theoretical model, 'Pulse Shape 2' (PS2), generated three-stage profile, derived from transforming the theoretical efficiency optimized output resistance function with the resistance profile.

resistance' profile was then used in this model to provide the input PWM signal for the Arduino to appropriately control the MOSFET to apply the desired circuit resistance function. For each optimized current pulse shape, the model generated theoretical exit velocities (for a given projectile at a given starting position) based on the position and displacement dependent force applied to the projectile.

The energy stored in a magnetic field (W) (where P is the power in Watts) is [9]

$$W = \int P\,dt = \frac{1}{2}lI(t)^2 \tag{5}$$

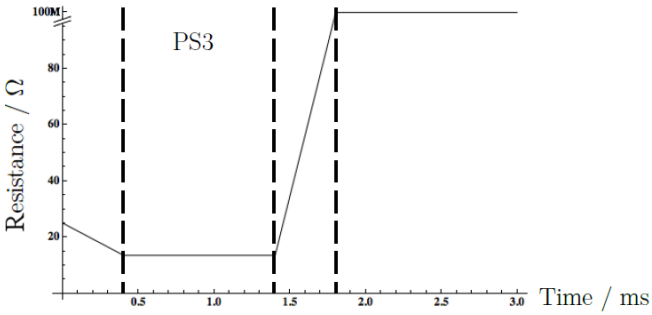

FIGURE 13. Theoretical model, 'Pulse Shape 3' (PS3), generated three-stage profile, derived from transforming the theoretical efficiency optimized output resistance function with the resistance profile.

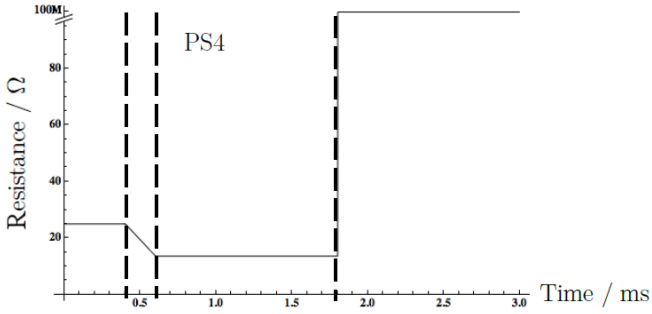

FIGURE 14. Theoretical model, 'Pulse Shape 4' (PS4), generated three-stage profile, derived from transforming the theoretical efficiency optimized output resistance function with the resistance profile.

Substituting

$$1 = \frac{\Re(x)\emptyset(\mathrm{x,\,t})^2}{\mathrm{I(t)}^2} \tag{6}$$

into Eq (4) gives

$$W = \frac{1}{2}\Re(x)\emptyset(x,t)^2 \tag{7}$$

Using the general equation for force;

$$F = \frac{\partial}{\partial x}W \tag{8}$$

and remembering that

$$\emptyset\,(x,t) = \frac{mmf\,(t)}{\Re(x)} = \frac{NI(t)}{\Re(x)} \tag{9}$$

Then;

$$F\,(x,t) = \frac{1}{2}N^2I(t)^2\frac{\partial}{\partial x}\left(\frac{1}{\Re(x)}\right) \tag{10}$$

To introduce a time-dependent resistance, using Eq. 4 and

$$I_0 = V_0/R(t) \tag{11}$$

(where $R(t)$ is the time-dependent resistance) gives

$$F(x,t) = \frac{1}{2}N^2\frac{V_0^2}{R\,(t)^2}e^{-\frac{2t}{RC}}\frac{\partial}{\partial x}\left(\frac{1}{\Re(x)}\right) \tag{12}$$

where $\phi(x,t)$ and $F(x,t)$ are the magnetic flux and the force applied to the projectile at position x and time t, V_0 is the

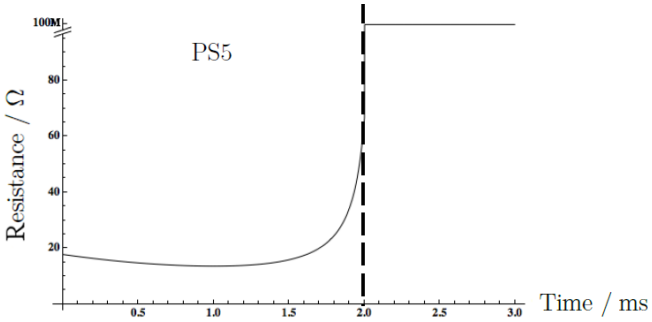

FIGURE 15. Theoretical model, 'Pulse Shape 5' (PS5), generated three-stage profile, derived from transforming the theoretical efficiency optimized output resistance function with the 'effective resistance' profile.

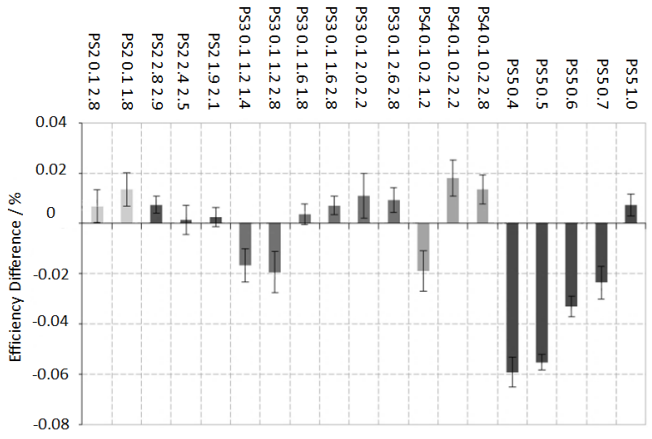

FIGURE 16. The change in efficiency of the reluctance accelerator system as a result of pulse shaping of the output current pulse on the drive coil. The efficiency difference is taken from the 'baseline' efficiency of the system (0.32±0.02)% without pulse shaping. The maximum efficiency increase was found to be for PS4 0.1 0.2 2.2 with an efficiency increase of 5.7% over the 'baseline' efficiency.

initial capacitor p.d. at time = 0s, R is minimum resistance of the system, C is the capacitance of the drive capacitor and $\Re(x)$ is the position dependent reluctance.

The following figures (Fig. 11–15) shows the theoretical efficiency optimized input PWM duty-cycle profiles from the theoretical model related to the system parameters.

The modelled resistance functions (Fig. 11–15) were then processed and flashed to the Arduino as an integer array to actively switch the MOSFET during capacitor discharge. For the experimental discharge circuit configuration, the minimum resistance was 11.2Ω. This equated to a 100% duty cycle for the PWM signal.

As the 'effective resistance' profile provided only a 'best fit' transfer function between the input Arduino function to the output resistance function of the discharge circuit, the durations between each stage of the input functions (highlighted by dashed lines in figures 11–15) were altered to maximize efficiency gains from pulse shaping. The pulse shape durations are denoted as, for example, PS3 0.1 1.2 1.4. This represents 'Pulse Shape 3' containing three pulse stages with boundaries at 0.1ms, 1.2ms and 1.4ms. Fig.16 shows the efficiency difference from the 'baseline' efficiency of a variety of durations for each pulse shape.

From Fig.16, a number of the new pulse shapes fail to increase the efficiency of the reluctance accelerator, particularly for PS5. The maximum efficiency achieved by the pulse shaping method was an increase of 5.7% over the unmodified current pulse ('baseline' efficiency) and 2% greater than that achieved by current pulse truncation only.

It must be noted that this accelerator system is far from an optimal configuration. Despite this, significant improvements in efficiency were achieved for this inherently inefficient device. The work demonstrated that pulse shaping can, indeed, increase reluctance accelerator performance. Future work will investigate the general optimization of the coil system to minimize magnetic losses in the flux-closure system and also will extend the work to see how pulse shaping can be applied to multistage accelerators.

REFERENCES

[1] G. W. Slade, "A simple unified physical model for a reluctance accelerator," *IEEE Trans. Magn.*, vol. 41, no. 11, pp. 4270–4276, Nov. 2005.
[2] D. A. Bresie and J. A. Andrews, "Design of a reluctance accelerator," *IEEE Trans. Magn.*, vol. 27, no. 1, pp. 623–627, Jan. 1991.
[3] A. Waindok and G. Mazur, "A mathematical and physical models of the three-stage reluctance accelerator," in *Proc. 2nd Int. Students Conf. Electrodyn. Mechatron. (SCE)*, May 2009, pp. 29–30.
[4] H. Xiang, B. Lei, Z. Li, and K. Zhao, "Design and experiment of reluctance electromagnetic launcher with new style armature," in *Proc. 16th Int. Symp. Electromagn. Launch Technol. (EML)*, Beijing, China, May 2012, pp. 1–4.
[5] S.-B. Liao, P. Dourmashkin, and J. Belcher, *Introduction to Electricity and Magnetism*. New York, NY, USA: Prentice-Hall, 2011.
[6] K. K. Tan, T. H. Lee, H. F. Dou, S. J. Chin, and S. Zhao, "Precision motion control with disturbance observer for pulsewidth-modulated-driven permanent-magnet linear motors," *IEEE Trans. Magn.*, vol. 39, no. 3, pp. 1813–818, May 2003.
[7] *ATmega48/88/168 Datasheet Rev. 2545T-AVR-05/11*, Atmel Corp., San Jose, CA, USA, 2011.
[8] A. P. Godse and U. A. Bakshi, *Electronic Devices and Circuits*, 1st ed. Maharashtra, India: Technical Pub., Jan. 2009, pp. 3–58.
[9] G. R. Slemon, *Electric Machines and Drives*. Reading, MA, USA: Addison-Wesley, 1992.